

## Systematics of the giant monopole resonance from inelastic alpha scattering

D. H. Youngblood, P. Bogucki, J. D. Bronson, U. Garg, Y.-W. Lui, and C. M. Rozsa\*

Cyclotron Institute, Texas A&M University, College Station, Texas 77843

(Received 8 October 1980)

The properties of the isoscalar giant monopole resonance have been studied with inelastic  $\alpha$  scattering between  $0^\circ \leq \theta_L \leq 8^\circ$ , where the quadrupole and monopole states can be distinguished by their angular distributions. Data were taken for  $^{12}\text{C}$ ,  $^{27}\text{Al}$ ,  $^{40}\text{Ca}$ ,  $^{48}\text{Ti}$ ,  $^{58}\text{Ni}$ ,  $^{64,66}\text{Zn}$ ,  $^{90}\text{Zr}$ ,  $^{116,118,120,124}\text{Sn}$ ,  $^{144,154}\text{Sm}$ , and  $^{208}\text{Pb}$  mostly at  $E_\alpha = 129$  MeV; some data were taken at  $E_\alpha = 99$  MeV and  $E_\alpha = 117$  MeV. A monopole resonance was identified in all the nuclei with  $A \geq 64$  at  $E_x \approx 76/A^{1/3}$  MeV. In nuclei with  $A \geq 90$ , most of the energy weighted sum rule was located in this state; in  $^{64,66}\text{Zn}$ , less than one-third of the energy weighted sum rule was located. No evidence for a monopole resonance was found in nuclei with  $A \leq 58$ .

NUCLEAR REACTIONS  $^{12}\text{C}$ ,  $^{27}\text{Al}$ ,  $^{40}\text{Ca}$ ,  $^{48}\text{Ti}$ ,  $^{58}\text{Ni}$ ,  $^{64,66}\text{Zn}$ ,  $^{90}\text{Zr}$ ,  $^{116,118,120,124}\text{Sn}$ ,  $^{144,154}\text{Sm}$ ,  $^{208}\text{Pb}(\alpha, \alpha')$ ;  $E_\alpha = 99, 117, 129$  MeV. Measured  $E_x$ ,  $\sigma(\theta)$ , giant resonances; deduced  $L$ , nuclear incompressibility.

### I. INTRODUCTION

Despite the intense study of giant resonances (GR) with a number of probes begun in 1970 when the giant quadrupole resonance (GQR) was identified, evidence for the giant monopole resonance (GMR) was elusive. In 1975, Marty *et al.*<sup>1</sup> suggested that differences in inelastic deuteron data and inelastic alpha spectra might be due to a GMR located just above the GQR in  $^{40}\text{Ca}$ ,  $^{90}\text{Zr}$ , and  $^{208}\text{Pb}$ . Analyses of electron scattering data by the Sendai group<sup>2</sup> showed that in  $^{90}\text{Zr}$  and  $^{208}\text{Pb}$ , the giant dipole resonance (GDR) strength estimated from the Steinwedel-Jensen model exhausts all of the ( $e, e'$ ) experimental strength in this region. The GDR strength estimated from the Goldhaber-Teller model is much smaller, however, and through the use of this model, the data are nicely fitted by a combination of the GDR and the GMR which essentially exhausts the full sum-rule strength. At Gröningen, Harakeh *et al.*,<sup>3</sup> utilizing inelastic alpha scattering, showed the existence of a second isoscalar component in several nuclei on the higher energy side of the peak thought to be the GQR. The angular distributions of this component were compatible with  $L=0$  or  $L=2$ .

Unambiguous identification of the GMR came from small-angle measurements of inelastic  $\alpha$  scattering<sup>4</sup> in which the upper component of the isoscalar GR peak in  $^{144}\text{Sm}$  and  $^{208}\text{Pb}$  was identified as  $L=0$  from the sharp dip apparent at very forward angles in the angular distributions. In extensions of this work,<sup>5,6</sup> the GMR has been reported in  $^{64}\text{Zn}$ ,  $^{66}\text{Zn}$ ,  $^{90}\text{Zr}$ , and  $^{116}\text{Sn}$ .

In a reanalysis of existing ( $p, p'$ ) data, Bertrand *et al.*,<sup>7</sup> utilizing revised estimates of the isovector part of the proton-nucleus interaction, have extracted parameters for a GMR at approximately

the position of the GDR in  $^{208}\text{Pb}$ ,  $^{144}\text{Sm}$ ,  $^{120}\text{Sn}$ ,  $^{90}\text{Zr}$ , and  $^{58}\text{Ni}$ , but they have reported no evidence for the GMR in  $^{40}\text{Ca}$ . The GDR and GMR could not be separated in this work, however, and the GMR could not be definitely identified from its angular distribution. The GMR has been observed and the multipolarity assignment confirmed in  $^{90}\text{Zr}$  and  $^{208}\text{Pb}$  in small-angle inelastic  $^3\text{He}$  scattering<sup>8</sup> and in  $^{90}\text{Zr}$ ,  $^{120}\text{Sn}$ , and  $^{208}\text{Pb}$  in small-angle deuteron scattering.<sup>9</sup>

The GMR is of interest both because it is one of a family of large-scale collective nuclear vibrations and because it leads directly to a property of nuclear matter not otherwise easily obtainable. There are three important quantities which characterize nuclear matter. Two are readily obtainable: the binding energy per particle from the semiempirical mass formula and the central density (or Fermi momentum) from electron scattering of heavy nuclei. The compression modulus (or incompressibility) of nuclear matter, however, can be obtained with any reasonable accuracy only from the energy of the GMR.

The incompressibility  $K_{\text{nm}}$  of nuclear matter is defined by<sup>10</sup>

$$K_{\text{nm}} = k_f^2 \frac{d^2}{dk_f^2} \left( \frac{E}{A} \right). \quad (1)$$

For a finite nucleus, the incompressibility can be defined similarly as

$$K_A = r_0^2 \frac{d^2(E/A)}{dr_0^2}. \quad (2)$$

$K_A$  can be related to the energy of the isoscalar GMR by<sup>10,11</sup>

$$E_M = \hbar/r_0 (K_A/m)^{1/2}, \quad (3)$$

where  $m$  is the nucleon mass.

The incompressibility of a finite nucleus differs from that of nuclear matter by surface, Coulomb, and symmetry effects. By use of the Weisacker expression for  $E/A$  in Eq. (2),  $K_A$  can be parametrized as<sup>10</sup>

$$K_A = K_{\text{vol}} + K_{\text{surf}} A^{-1/3} + K_{\text{sym}} \left( \frac{N-Z}{A} \right)^2 + K_{\text{Coul}}, \quad (4)$$

where  $K_{\text{vol}}$  is usually identified as  $K_{\text{nm}}$ . The coefficients in Eq. (4) can be viewed as second derivatives with respect to  $r$  of corresponding coefficients in the mass equation. Unfortunately, the derivatives of the coefficients in the mass equation cannot be evaluated with sufficient accuracy to determine  $K_{\text{sym}}$  or  $K_{\text{surf}}$ . However, these coefficients of incompressibility can be obtained from Eq. (4) if the position of the GMR is known over a wide range of  $A$  and  $Z$ .

In order to ascertain the systematics of the GMR and to obtain sufficient data to establish the incompressibility coefficients from Eq. (4), we have utilized small-angle inelastic  $\alpha$  scattering in an attempt to identify the GMR and obtain its parameters in fifteen nuclei between  $^{12}\text{C}$  and  $^{208}\text{Pb}$ . Results for several of the nuclei have already been published.<sup>4-6</sup>

## II. EXPERIMENTAL TECHNIQUE AND DATA ANALYSIS

Because of the highly absorptive nature of the  $\alpha$ -nucleus interaction, the gross features of the angular distributions expected in inelastic  $\alpha$  scattering can be seen by use of the diffraction (or Blair) model. The cross section is given<sup>12</sup> by the square of a Bessel function ( $J_n$ ) and has the forms

$$\left( \frac{d\sigma}{d\Omega} \right)_{0^+ \rightarrow 0^+} \propto |J_0(qR_D)|^2, \quad (5)$$

$$\left( \frac{d\sigma}{d\Omega} \right)_{0^+ \rightarrow 1^+} \propto |J_1(qR_D)|^2, \quad (6)$$

$$\left( \frac{d\sigma}{d\Omega} \right)_{0^+ \rightarrow 2^+} \propto \left[ \frac{1}{4} J_0^2(qR_D) + \frac{3}{4} J_2^2(qR_D) \right]. \quad (7)$$

Here,  $q$  is the momentum transfer, and  $R_D$ , the diffraction radius, is adjusted to fit the phase of the elastic scattering angular distribution. A schematic calculation with Eqs. (5) and (7) is shown in Fig. 1, where  $R_D$  has been adjusted to fit elastic scattering. Transitions involving odd multiplicities are out of phase with those involving even multiplicities; furthermore, at large angles the phase of the angular distribution is the same for all even (odd) multiplicities. As can be seen in Ref. 12, experimental data follow these predictions closely. This simple model suggests

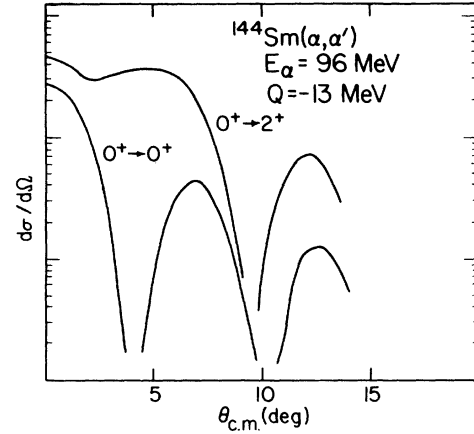


FIG. 1. Diffraction model predictions.

that the GQR and GMR can be distinguished at  $E_\alpha \approx 100$  MeV by measurements over the angular range  $3^\circ \leq \theta \leq 8^\circ$  and that the maximum enhancement of the GMR will occur at  $0^\circ$ . Also, the GQR and GMR should be easily distinguishable from the GDR (which is, in any case, only weakly excited by the isoscalar  $\alpha$  particle).

Distorted-wave Born approximation (DWBA) calculations of  $(\alpha, \alpha')$  angular distributions expected for the isoscalar GMR, GQR, the hexadecapole resonance, and the isovector GDR in  $^{144}\text{Sm}$  are shown in Fig. 2. The curves correspond to the full energy weighted sum rule (EWSR) for each. The techniques used in the calculation are described in Ref. 5. It is clear that the DWBA calculation has preserved the features of the Blair

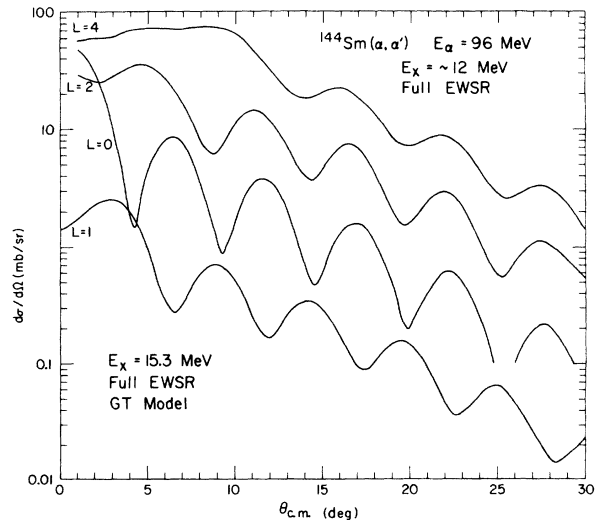


FIG. 2. DWBA prediction for inelastic  $\alpha$  scattering from  $^{144}\text{Sm}$ . The  $L=0, 2, 4$  calculations are for  $E_x \approx 12$  MeV while the  $L=1$  calculation is for  $E_x = 15.3$  MeV.

model. Furthermore, it is apparent that the GMR is weakly excited relative to the other isoscalar states in this reaction except near  $0^\circ$ . GDR excitation should be negligible except at the minima in the GMR.  $^{12}\text{C}(\alpha, \alpha')$  angular distributions obtained for  $0^\circ \leq \theta \leq 20^\circ$  for excitation of  $2^+$ ,  $0^+$ , and  $3^-$  states are shown in Fig. 3. The data for the  $0^+$  state do indeed show the expected sharp dip, while the data for the  $2^+$  (and  $3^-$ ) states are quite flat. The shapes are reproduced reasonably well by DWBA predictions. The calculation for the  $0^+$  state assumed a breathing mode form factor (see Ref. 5) and reproduces the data for the 7.6 MeV state fairly well, although excitation of this state in  $(p, p')$  has been best fit by a two-step process.<sup>13</sup>

The inelastic  $\alpha$ -scattering measurements at small angles should provide a reliable identification of the GMR, while data near  $0^\circ$  provide the maximum enhancement of the GMR relative to the GQR which, in principle, offers the most accurate GMR parameters. The experimental techniques for such measurements, including data reduction and DWBA calculations, have been described in detail in Ref. 5 and are discussed only briefly here.

Alpha-particle beams from the Texas A&M cyclotron bombarded self-supporting targets placed at the center of the target chamber for the Enge split-pole magnetic spectrograph. All of the targets contained  $>95\%$  of the desired isotope. Inelastically scattered alpha particles were detected over an outgoing energy range of approximately 50 MeV in the focal plane of the spectrograph by an 86-cm-long resistive-wire proportional counter backed by an NE102 scintillator. Particle identification was accomplished using total-energy and time-of-flight signals obtained from the scintillator and energy-loss signals obtained from the proportional counter. These signals were routed to a PDP-15 on-line computer, and sums, divisions, and pulse selections were

performed in real time. Considerable care was taken to minimize background contributions from various secondary scatterings, and an energy resolution of  $\approx 300$  keV, primarily due to straggling in the target, was obtained. A solid-state detector, placed at  $\approx 20^\circ$  in the scattering chamber, was used to monitor the beam integration, and a pulser signal was fed through the signal manipulation circuits and the computer to determine the intrinsic dead time of the system. Cross sections were obtained from the known target thickness, solid angle, and beam charge, including the appropriate dead-time corrections.

Because the structure in the angular distributions moves to smaller angles as the bombarding energy is increased, early measurements were made below 100 MeV where the first minimum in the  $L=0$  angular distributions occurs at  $\theta_L \geq 4^\circ$ . This permitted the observation of this cross-section minimum. However, both the ratio of GMR to GQR and GMR to continuum yields increase with increasing energy; therefore, when the  $0^\circ$  measurements were perfected, all subsequent measurements were done at 129 MeV (the highest energy beam available). One Ca run was performed at 117 MeV.

### III. EXPERIMENTAL RESULTS AND DISCUSSION

Inelastic  $\alpha$ -scattering data were taken over the angular range  $0^\circ \leq \theta_L \leq 8^\circ$  on fifteen targets, ranging from  $^{12}\text{C}$  to  $^{208}\text{Pb}$ , in order to identify the GMR and to ascertain its properties for a wide range of nuclei. The targets, beam energies, and the angles at which data were obtained for individual targets are summarized in Table I. A sample of the spectra obtained is shown in Figs. 4 and 5. For heavier targets, such as Sm and Pb, secondary scattering from the solid-angle defining slits produced a continuum background discernible in the spectra for  $\theta_L \leq 5^\circ$ , and measurements below  $3^\circ$  were practical only at  $0^\circ$  where spectra were obtained with a significantly larger solid angle. At  $0^\circ$ , slit-scattering contributions were clearly evident only for targets with  $Z \geq 60$ . For  $^{40}\text{Ca}$ , the GR was discernible at  $2^\circ$  and quite prominent at  $3^\circ$ .

A multiple-peak fitting routine was used to fit the data after subtraction of the continuum to determine the parameters of the GQR and GMR. A sample of two-peak fits to  $^{124}\text{Sn}$  data is shown in Fig. 6. Two Gaussians shown superimposed on the data were fitted simultaneously to the giant resonance peaks in the spectra for all angles measured by use of a least-squares technique.<sup>14</sup> Uncertainties in the peak parameters (centroid, width, and amplitude), which correspond to the

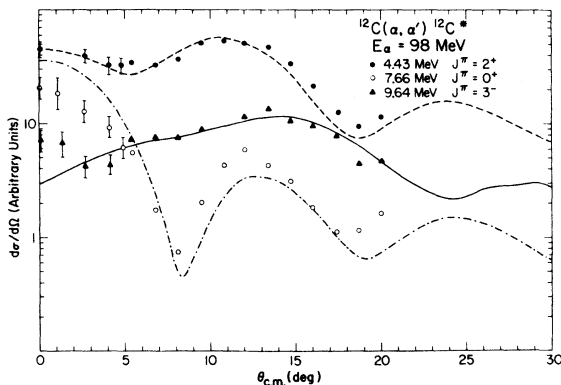


FIG. 3.  $^{12}\text{C}(\alpha, \alpha')$  angular distributions. The curves are DWBA predictions for the appropriate  $L$  transfers.

TABLE I. Targets, energies, and angles at which spectra were obtained for individual targets.

Target	$E_\alpha$ (MeV)	$\theta_L$ (deg)
$^{12}\text{C}$	129	0, 2, 3, 4, 5, 6, 7, 8
$^{27}\text{Al}$	129	0, 6
$^{40}\text{Ca}$	99	3, 3.5, 4, 4.5, 5, 6, 7, 8
	117	2, 2.5, 3, 3.5, 4, 4.5, 5, 6, 7, 8
	129	0, 4
$^{48}\text{Ti}$	98	2, 2.5, 3, 4, 5, 6, 7
$^{58}\text{Ni}$	129	0, 3, 3.5, 4, 4.5, 5, 6, 7
$^{64}\text{Zn}$	129	0, 2.5, 3, 3.5, 4, 4.5, 5, 6
$^{66}\text{Zn}$	129	0, 3, 3.5, 4, 4.5, 5, 6
$^{90}\text{Zr}$	96	0, 3, 3.5, 4, 4.5, 5, 6, 7
	129	0, 4
$^{116}\text{Sn}$	129	0, 3, 3.5, 4, 5, 6, 7
$^{118}\text{Sn}$	129	0, 4, 6
$^{120}\text{Sn}$	129	0, 4
$^{124}\text{Sn}$	129	0, 3, 4, 5, 6
$^{144}\text{Sm}$	96	3, 3.5, 4, 4.5, 5, 6, 7
	129	0, 4
$^{154}\text{Sm}$	97	3, 3.5, 4, 4.5, 5, 6, 7
	129	0, 3, 3.5, 4, 4.5, 5, 6
$^{208}\text{Pb}$	99	3, 3.5, 4, 4.5, 5, 6, 7
	129	0, 2.5, 3.5, 4, 5, 6

variance or mean square deviation of those parameters, were obtained from appropriate elements of the error matrix. The parameters for all the nuclei studied are summarized in Table II; the excitation energy and width uncertainties include background, energy calibration, and peak decomposition ambiguities. The GQR parameters reported herein differ somewhat from our earlier results<sup>15</sup> primarily because the parameters reported in Ref. 15 were obtained by fitting the GR region by a single broad peak, all of which was assumed to be the GQR. The  $L=0$  sum-rule percentages obtained for the Sn isotopes are relatively high compared to the other nuclei, although they do overlap within error limits. These high sum-rule values might be attributed to the failure of DWBA calculations in correctly reproducing the beam-energy dependence of the predicted cross sections. Additionally, it should be noted that the introduction of a small asymmetry in the shape of the dominant GQR component will reduce the  $L=0$  strength considerably, without any significant effect on the quality of the overall fits. The angular distributions obtained for many of the nuclei are shown along the DWBA predictions in Fig. 7. The error bars on the data points are the mean-square deviation and, hence, do not account for uncertainties in the choice of background. The uncertainties in the absolute cross sections are quite large because of uncertainties in background and peak decomposition. As pointed

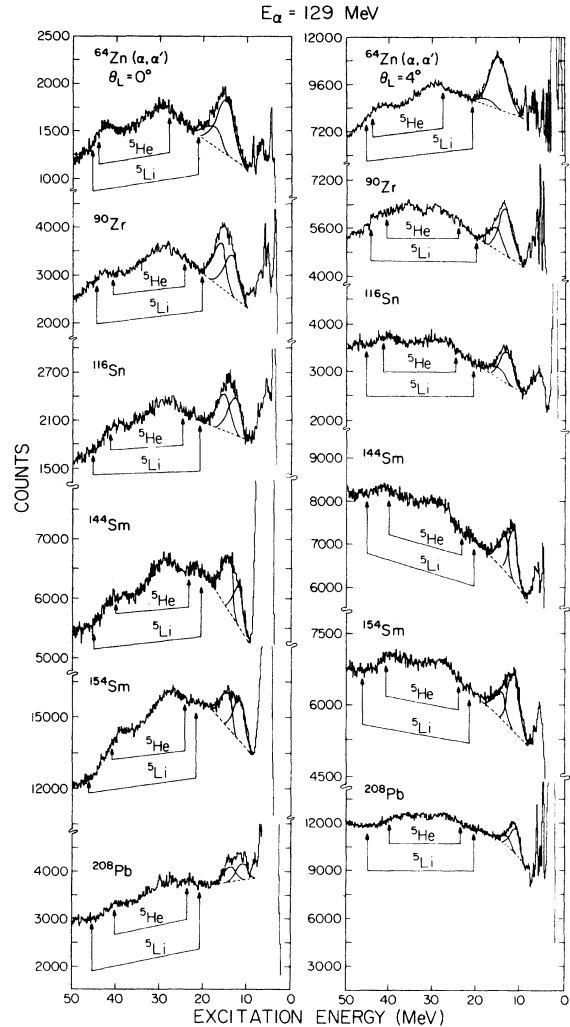


FIG. 4. Inelastic  $\alpha$  spectra obtained at  $0^\circ$  and  $4^\circ$ . The GQR and GMR peaks and the background on which they reside are indicated. The regions where  $^5\text{He}$  and  $^5\text{Li}$  breakup would contribute are also indicated.

out earlier, the GMR yield obtained is sensitive to the shape of the GQR, and the analyses which assume that the GQR has a high-energy tail result in acceptable fits which produce GMR yields that are as much as a factor of 3 smaller than for a symmetric GQR.

A GMR exhausting a large fraction of the sum rule is apparent in nuclei with  $A \geq 90$ . For  $^{64,66}\text{Zn}$ , the higher excitation component is quite weak and accounts for only about 30% of the isoscalar  $E0$  EWSR. The large errors on  $E_x$  and  $\Gamma$  for the monopole peak in the Zn isotopes reflect the sensitivity of the parameters to different background assumptions and differing GQR parameters. The energy and width systematics of the GMR are illustrated in Fig. 8. Of particular interest is the behavior<sup>16</sup> of the components of the GR peak

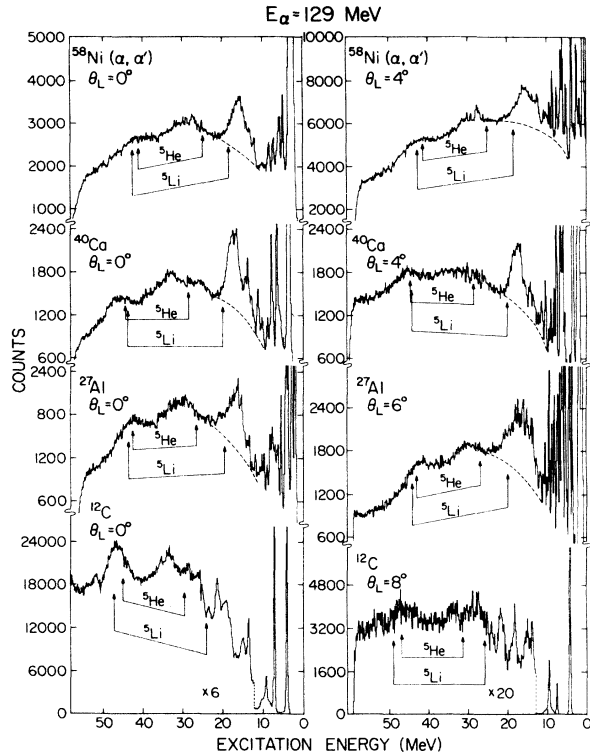


FIG. 5. Inelastic  $\alpha$  spectra. The choice of continuum is indicated by a dashed line. The regions where  ${}^5\text{He}$  and  ${}^5\text{Li}$  breakup would contribute are also indicated.

in deformed  ${}^{154}\text{Sm}$  relative to spherical  ${}^{144}\text{Sm}$ . In  ${}^{154}\text{Sm}$ , the GQR is substantially broader, there is an increased energy separation between the GQR and the GMR, and the GMR strength is apparently

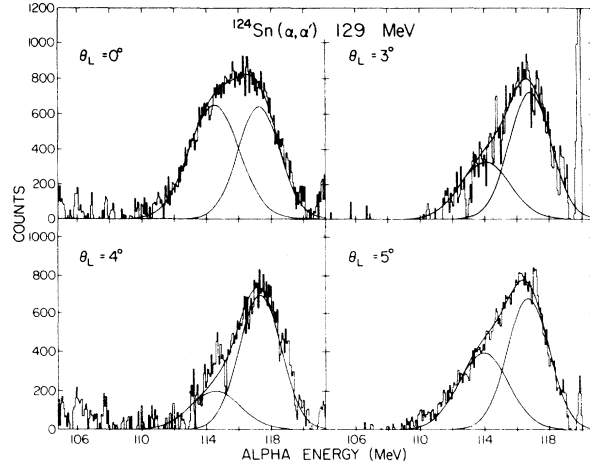


FIG. 6. Portions of spectra for  ${}^{124}\text{Sn}$  taken at angles indicated. The continuum has been subtracted. Two peak fits and their sums are shown superimposed.

split into two components. That these effects result from the deformation of the nuclear ground state is clear if one contrasts the Sm results with those for the Sn isotopes, as discussed below.

The GMR and GQR were studied in four Sn isotopes to observe their behavior in an isotopic series which does not involve substantial change in ground-state shape. The behavior of  $E_x A^{1/3}$  and  $\Gamma$  for the GMR and GQR as a function of  $A$  is illustrated for the Sn isotopes in Fig. 9. Within the errors, each is constant over this isotopic series. As expected, the GQR width, the difference in GQR and GMR energies, and the EWSR fractions remain essentially constant, in contrast

TABLE II. Parameters obtained for giant resonance peaks from small-angle inelastic scattering.

Nucleus	$E_x$ (MeV)	GQR		EWSR (%)	$E_x$ (MeV)	GMR		$K_A$ (MeV)
		$\Gamma$ (MeV)				$\Gamma$ (MeV)	EWSR (%)	
${}^{12}\text{C}$		not observed				not observed		
${}^{27}\text{Al}$	$20.1 \pm 0.3$	$7.6 \pm 0.3$				not observed		
${}^{40}\text{Ca}$	$17.7 \pm 0.3$	$2.5 \pm 0.4^a$		$48 \pm 8$		not observed		
${}^{48}\text{Ti}$	$16.2 \pm 0.4$	$4.5 \pm 0.5$				not observed		
${}^{58}\text{Ni}$	$16.4 \pm 0.3$	$4.9 \pm 0.2$		$55 \pm 15$		not observed		
${}^{64}\text{Zn}$	$15.3 \pm 0.3$	$4.7 \pm 0.4$		$38 \pm 10$	$18.2 \pm 0.5$	$4.3 \pm 0.9$	$29 \pm 16$	$116 \pm 10$
${}^{66}\text{Zn}$	$14.9 \pm 0.5$	$4.5 \pm 0.5$		$38 \pm 10$	$18.4 \pm 0.7$	$4.1 \pm 1.1$	$30 \pm 16$	$122 \pm 20$
${}^{90}\text{Zr}$	$14.0 \pm 0.2$	$3.4 \pm 0.2$		$66 \pm 17$	$16.2 \pm 0.5$	$3.5 \pm 0.3$	$90 \pm 20$	$116 \pm 7$
${}^{116}\text{Sn}$	$13.2 \pm 0.2$	$3.3 \pm 0.2$		$84 \pm 25$	$15.6 \pm 0.3$	$4.1 \pm 0.3$	$180 \pm 60$	$128 \pm 5$
${}^{118}\text{Sn}$	$13.2 \pm 0.3$	$3.5 \pm 0.3$		$\approx 60$	$15.5 \pm 0.6$	$4.1 \pm 0.7$	$\approx 150$	$127 \pm 10$
${}^{120}\text{Sn}$	$12.7 \pm 0.4$	$3.5 \pm 0.4$		$\approx 80$	$15.2 \pm 0.5$	$4.1 \pm 0.6$	$\approx 180$	$124 \pm 10$
${}^{124}\text{Sn}$	$12.3 \pm 0.4$	$3.1 \pm 0.3$		$78 \pm 25$	$14.8 \pm 0.4$	$3.8 \pm 0.6$	$186 \pm 60$	$120 \pm 6$
${}^{144}\text{Sm}$	$12.2 \pm 0.2$	$2.4 \pm 0.2$		$45 \pm 15$	$14.6 \pm 0.2$	$3.0 \pm 0.3$	$140 \pm 40$	$129 \pm 5$
${}^{154}\text{Sm}$	$11.8 \pm 0.3^b$	$3.7 \pm 0.3^b$		b	$14.9 \pm 0.3$	$2.6 \pm 0.4$	$55 \pm 15$	$141 \pm 11$
${}^{208}\text{Pb}$	$11.0 \pm 0.2$	$2.7 \pm 0.3$		$105 \pm 25$	$13.7 \pm 0.4$	$3.0 \pm 0.5$	$90 \pm 20$	$145 \pm 8$

<sup>a</sup> rms width.

<sup>b</sup> Contains a portion of the GMR (see text and Fig. 7).

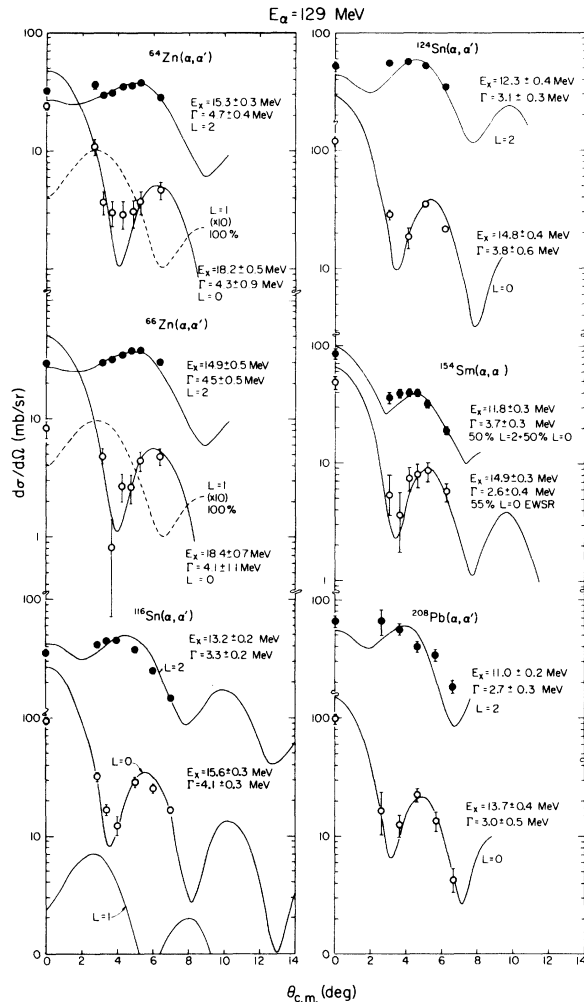


FIG. 7. Angular distributions obtained for GR peaks. DWBA fits are shown superimposed.

with the Sm isotopes.

So far, the identification of significant monopole strength in nuclei lighter than Zn has proved elusive. Extensive data have been acquired on several targets with  $A < 58$ ; the beam energies and angles at which spectra were taken for the various targets are summarized in Table I. For light targets, the peak corresponding to the breakup of  ${}^5\text{Li}$  contributes to the continuum near the upper side of the GR peak and increases somewhat the ambiguity of background choice. This is apparent in Fig. 5. Particular emphasis was placed on  ${}^{40}\text{Ca}$  and  ${}^{58}\text{Ni}$  since tentative evidence for a GMR in these nuclei has been reported previously.<sup>1,9</sup> The results of our  ${}^{40}\text{Ca}$  studies are reported more completely elsewhere.<sup>17</sup> Sample spectra taken for  ${}^{12}\text{C}$ ,  ${}^{27}\text{Al}$ ,  ${}^{40}\text{Ca}$ , and  ${}^{58}\text{Ni}$  are shown in Fig. 5. The GMR in these nuclei is not apparent from these spectra. The GR peaks after continuum subtrac-

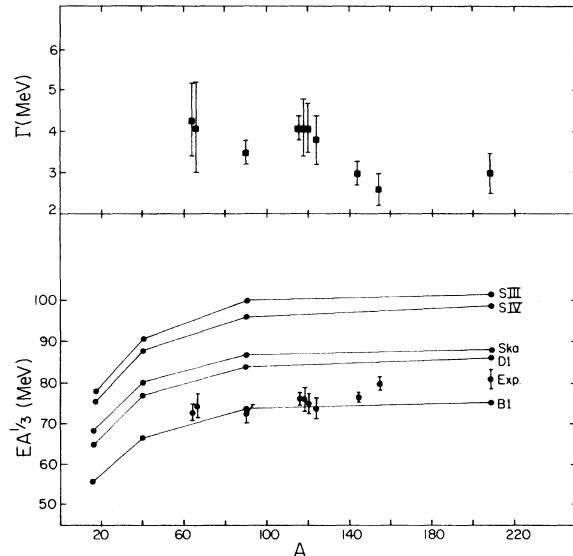


FIG. 8. Systematics of the GMR. RPA predictions of Blaizot *et al.* (Ref. 10) are also shown.

tion taken at  $0^\circ$ , where the GMR is a maximum, and angles where the GMR should be weak are shown for  ${}^{90}\text{Zr}$ ,  ${}^{64}\text{Zn}$ ,  ${}^{58}\text{Ni}$ ,  ${}^{40}\text{Ca}$ , and  ${}^{27}\text{Al}$  in Fig. 10. The monopole strength is obvious in the  $0^\circ$

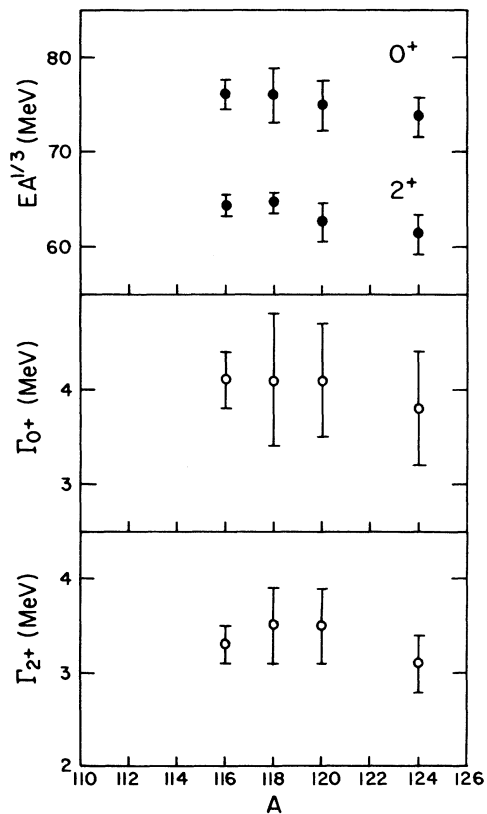


FIG. 9. Behavior of GR parameters in Sn isotopes.

data for  $^{90}\text{Zr}$  and can be seen in the  $^{64}\text{Zn}$  data, but in  $^{40}\text{Ca}$  and  $^{58}\text{Ni}$  the shape of the GR peak is virtually the same on the higher excitation energy side at  $0^\circ$  and  $4^\circ$ . In  $^{40}\text{Ca}$ , a sharp peak at  $E_x \approx$

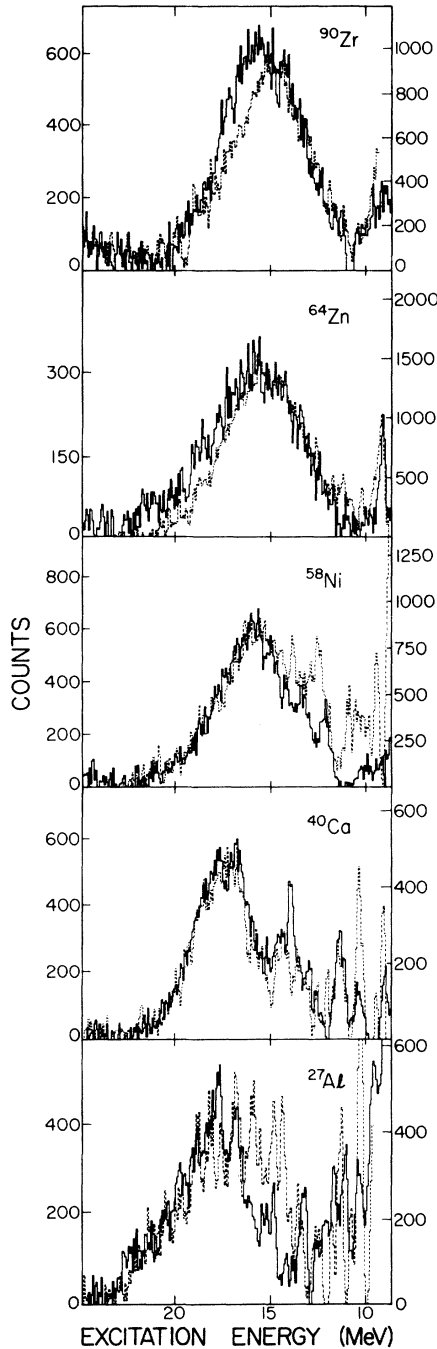


FIG. 10. Spectra in the GR region after continuum subtraction. The solid lines (left side scale) represent data taken at  $0^\circ$  where the GMR is maximum, while the dashed lines (right side scale) represent data taken at  $4^\circ$  (except, for  $^{27}\text{Al}$ , at  $6^\circ$ ) where the GMR is near a minimum.

14 MeV is strong at  $0^\circ$  but absent at  $4^\circ$ , suggesting a  $0^+$  assignment, although it contains only  $\approx 7\%$  of the  $E0$  EWSR. Angular distributions obtained for several different regions of the GR peak in  $^{40}\text{Ca}$  are shown in Fig. 11, and each is fit well by  $L=2$ . Groups at Orsay,<sup>9</sup> Grenoble,<sup>18</sup> and Erlangen<sup>19</sup> have also reported searches for the GMR in  $^{40}\text{Ca}$ , and their results suggest that the monopole strength is spread over a large energy region. An Osaka group earlier reported<sup>20</sup> a weak narrow  $0^+$  state at 14 MeV utilizing inelastic  $^3\text{He}$  scattering at  $1.2^\circ$ .

Bertrand *et al.*,<sup>7</sup> who utilized inelastic proton scattering, found no evidence for a monopole in  $^{40}\text{Ca}$  but reported  $30 \pm 10\%$  of the  $E0$  EWSR in a peak  $E_x = 19.8$  MeV with  $\Gamma = 3.5$  MeV in  $^{58}\text{Ni}$ . While this is very similar to our results for  $^{64},^{66}\text{Zn}$ , no such concentration of  $0^+$  strength in  $^{58}\text{Ni}$  could be identified from the small-angle inelastic  $\alpha$  scattering. The angular distributions obtained for different regions of the GR peak in  $^{58}\text{Ni}$  are shown in Fig. 12. While there might be some suggestion of monopole strength in the higher excitation regions of the peak, the region above 18 MeV is not dominated by  $0^+$  strength. Willis *et al.*<sup>9</sup> reported the possible presence of monopole strength in  $^{58}\text{Ni}$  coincident with the quadrupole strength, but they did not observe an identifiable monopole state, in

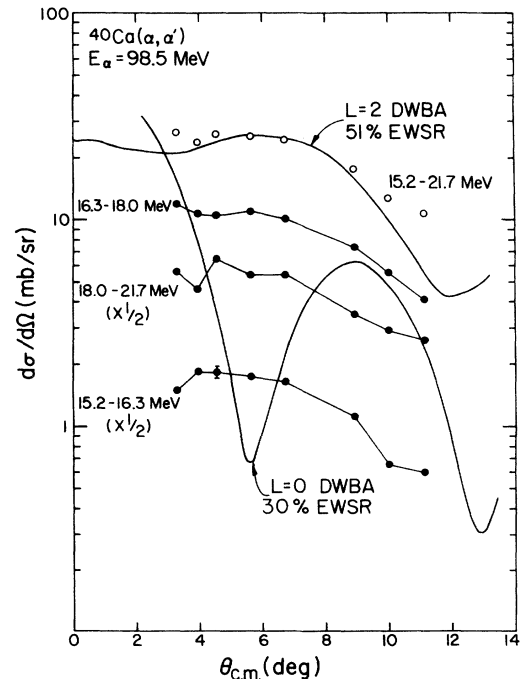


FIG. 11. Angular distributions obtained for different regions of the GR peak in  $^{40}\text{Ca}$ .  $L=0$  and  $2$  DWBA predictions are shown superimposed. The error bar shown is representative of the statistical errors.

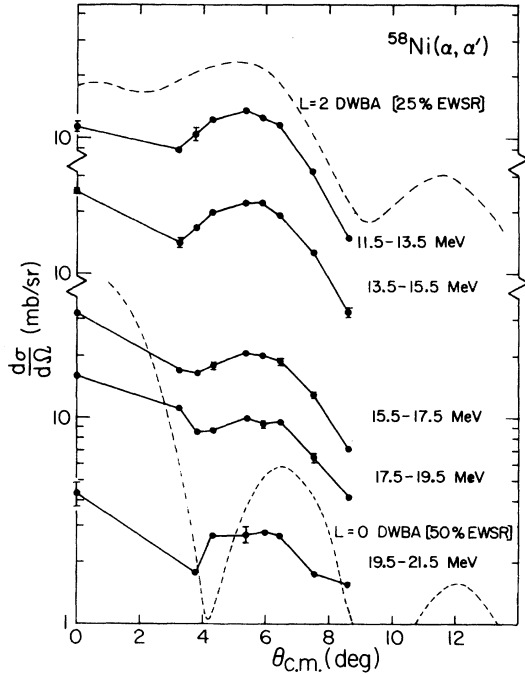


FIG. 12. Angular distributions obtained for different regions of the GR peak in  $^{58}\text{Ni}$ .  $L=0$  and 2 DWBA predictions corresponding to the indicated EWSR strengths are shown superimposed. A few representative error bars are shown; they correspond to statistical errors only.

disagreement with the results of Bertrand *et al.*<sup>7</sup>

The shape of the GR peak in  $^{27}\text{Al}$  is quite different at  $0^\circ$  and  $6^\circ$ , but no concentration of strength is apparent at  $0^\circ$  which is absent at  $6^\circ$ . From large-angle data,<sup>21</sup> it is clear that the peak contains several multipolarities, particularly in the fine structure. In  $^{12}\text{C}$ , in addition to the 7.655 MeV  $0^+$  state, a broad ( $\Gamma \approx 2.5$  MeV) state is observed at  $E_x = 10.3 \pm 0.3$  MeV which is most intense at  $0^\circ$  and has an angular distribution consistent with a  $0^+$  assignment; this latter state can be identified as the previously known<sup>22</sup> state at 10.3 MeV. By fitting the bump under the 9.6 MeV peak with two Gaussians, Buenerd *et al.*<sup>23</sup> have reported an  $L=0$  state at 9.15 MeV. While we do observe this peak in the  $0^\circ$  data, it is extremely weak at other angles, and it is not possible to reach any definitive conclusions regarding its character. Data were obtained on  $^{48}\text{Ti}$  at  $E_\alpha = 99$  MeV over the range from  $2^\circ$  to  $8^\circ$ . A sample spectrum and the angular distribution obtained for the entire GR peak are shown in Fig. 13. The angular distribution is fit well by an  $L=2$  DWBA calculation. However, these  $^{48}\text{Ti}$  data were the first small-angle data taken here, and no absolute normalization was obtained; hence the strength of the GQR could not be obtained. In an attempt to iden-

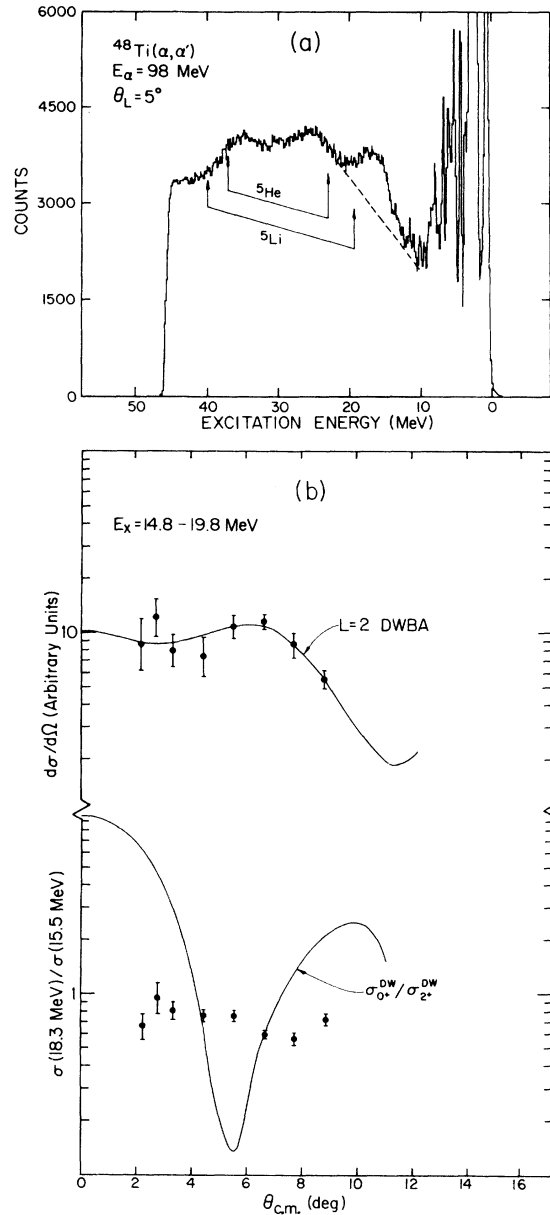


FIG. 13. (a) Inelastic  $\alpha$  spectrum for  $^{48}\text{Ti}$ ; the dashed line represents the assumed continuum. (b) The angular distribution of the GR peak along with an  $L=2$  DWBA prediction is shown in the upper part. The lower part shows the ratio of cross sections for the upper and lower regions of the peak (see text); the DWBA prediction for  $\sigma_{0^+}/\sigma_{2^+}$  is shown superimposed.

tify the presence of monopole strength in the peak, analyses were performed for two regions,  $14.3 \leq E_x \leq 16.5$  MeV and  $16.6 \leq E_x \leq 19.7$  MeV. The ratio of the cross sections for the lower and upper regions is also plotted in Fig. 13 along with  $\sigma_{0^+}^{DW}/\sigma_{2^+}^{DW}$ , the ratio of DWBA predictions for a  $0^+$  and  $2^+$  state. As can be seen, the data for this ratio are quite flat. Thus, as in the case of  $^{40}\text{Ca}$

and  $^{58}\text{Ni}$ , the location of the GMR in  $^{48}\text{Ti}$  is not apparent. Some of the GMR parameters reported from different laboratories are tabulated in Table III. Generally, the results are in agreement within the errors. It should be noted, however, that several of the experiments were not able to distinguish the GMR from the GQR; in those cases, the data were assumed to consist of two peaks in the GR region, and parameters obtained for the peak at high excitation were associated with the GMR.

#### IV. CONCLUSIONS

The results of various random-phase approximation (RPA) calculations made by Blaizot *et al.*<sup>10</sup> are shown with the energy systematics of the GMR in Fig. 8. The data points lie in the region of the finite range predictions of the *B1* and *D1* interactions, resulting in  $K_{\text{nm}} \approx 200$  MeV which is well below the predictions of the pure Skyrme-type interactions. The incompressibility of infinite nuclear matter and the surface and symmetry contributions to incompressibility, which were determined from Eq. (4) with a least-squares fit to the values of  $K_A$  from Table II (excluding  $^{154}\text{Sm}$ ), are listed in Table IV. The values of nuclear incompressibility parameters obtained in the present calculation are slightly different from those in Ref. 6. This is due to the use of updated values of GMR energies for  $^{118}\text{Sn}$  and  $^{144}\text{Sm}$  and the use of  $K_A$  values obtained from the data in Table II only.  $K_{\text{nm}}$ ,  $K_{\text{surf}}$ , and  $K_{\text{sym}}$  obtained by

Blaizot *et al.* for three different interactions are also shown in Table IV. The results using the interactions *B1* of Brink and Boeker and *D1* of Gogny agree with the experimental data within the errors. The value of  $K_{\text{sym}}$  obtained with the *B1* and *D1* interactions is at the upper limit of the experimental error. We must caution, however, that it is appropriate to use the observed energy to obtain  $K_A$  only if the entire *E0* strength is located in the observed peak. This does not appear to be true for  $^{64,66}\text{Zn}$  within the errors.

Bohigas *et al.*<sup>11</sup> related the incompressibility of nuclear matter  $K_{\text{nm}}$  to that of a finite nucleus  $K_A$  by connecting the monopole and quadrupole energies through a schematic form of a Skyrme-type force. They obtained the simple relationship  $K_{\text{nm}} - K_A \approx 63(\gamma + 1)$ , where  $\gamma$  is the power of the density dependence of the Skyrme-type force. They showed that  $\gamma \approx \frac{1}{3}$  is required to reproduce both the GMR and GQR energies, leading to  $K_{\text{nm}} \approx 230$  MeV, which agrees reasonably well with the value we obtained from Eq. (4).

It has been suggested by Jennings *et al.*<sup>25</sup> that the value  $K_{\text{vol}}$  obtained from Eq. (4) does not correspond to the incompressibility of infinite nuclear matter ( $K_{\text{nm}}$ ) but, instead,  $K_{\text{vol}} = 0.7 K_{\text{nm}}$ . That would imply  $K_{\text{nm}} = 287 \pm 50$  MeV from our results. This is in disagreement with the value from Bohigas *et al.*,<sup>11</sup> as quoted above. Also, this value of  $K_{\text{nm}}$  is closer to the calculated  $K_{\text{nm}}$  for the *SIV* interaction in Ref. 10; however, the monopole energies calculated *SIV* are much higher than the experimental energies (see Fig. 8). These dis-

TABLE III. Comparisons of parameters for the GMR.

Nucleus	$E_x$ (MeV)	$\Gamma$ (MeV)	EWSR (%)	Reference
$^{90}\text{Zr}$	$16.2 \pm 0.5$	$3.5 \pm 0.3$	$90 \pm 20$	5
	$16.4 \pm 0.3$	$3.6 \pm 0.3$	60	8
	$17.2 \pm 0.5$	$4.3 \pm 0.3$	$25 \pm 8, 19 \pm 6$	9 <sup>a</sup>
	$17.5 \pm 0.5$	$3.0 \pm 0.5$	$60 \pm 25$	7
$^{120}\text{Sn}$	$15.2 \pm 0.5$	$4.1 \pm 0.6$	$\approx 180$	present work
	$16.1 \pm 0.4$	$4.0 \pm 0.4$	$64 \pm 15, 31 \pm 8$	9 <sup>a</sup>
	$16.8 \pm 0.5$	$3.5 \pm 0.5$	$100 \pm 25$	7
$^{144}\text{Sm}$	$14.6 \pm 0.2$	$3.0 \pm 0.3$	$140 \pm 40$	16
	$15.5 \pm 0.5$	$2.5 \pm 0.5$	$100 \pm 25$	7
$^{208}\text{Pb}$	$13.7 \pm 0.4$	$3.0 \pm 0.5$	$90 \pm 20$	4
	$13.2 \pm 0.3$	$2.8 \pm 0.3$	94	8
	$13.5 \pm 0.3$	$2.8 \pm 0.2$	$51 \pm 10, 307 \pm 60$	9 <sup>a</sup>
	$13.3 \pm 0.3$	$2.5 \pm 0.6$	$110 \pm 22$	3
	$13.4 \pm 0.3$	$3.0 \pm 0.5$	$90 \pm 25$	7
	$13.8 \pm 0.3$	$2.6 \pm 0.3$		24

<sup>a</sup> Sum-rule percentages extracted using two different optical-potential parameter sets.

TABLE IV. Coefficients of the incompressibility (MeV).

	Expt.	$B1^a$	$D1^a$	$Ska^a$
$K_{nm}$	$201 \pm 35$	190	228	263
$K_{surf}$	$-325 \pm 140$	-300	-315	-394
$K_{sym}$	$-59 \pm 275$	-500	-500	-610

<sup>a</sup> Theoretical values from Ref. 10 using the indicated interactions.

crepancies in the various theoretical approaches remain to be resolved.

The splitting of the GDR and the broadening of the GQR in permanently deformed nuclei are now well established. Naively, one would expect the GMR to be unaffected by the deformation of the ground state. But Zawischa *et al.*<sup>26</sup> have performed RPA calculations for several deformed nuclei which show a splitting of the isoscalar GMR into two components, one just below the GQR carrying about one-third of the strength and one 8 MeV higher in excitation carrying about two-thirds of the strength. However, the experimental data for spherical <sup>144</sup>Sm and deformed <sup>154</sup>Sm show a somewhat different picture.<sup>16</sup> In <sup>154</sup>Sm, the observed GMR cross section was about 50% of that in <sup>144</sup>Sm. This decrease in the GMR cross section corresponded almost exactly to the observed increase in the cross section of the lower excitation peak. Such an effect implies that the GMR has split into two components in <sup>154</sup>Sm and that one of these components coincides in excitation energy with the GQR.

This splitting is further corroborated by the observed increase in the difference between the excitation energies of the two peaks which are farther apart in <sup>154</sup>Sm. The apparent "splitting" of the GMR can be qualitatively understood by an extension of the model applied to the splitting of the GQR.<sup>27</sup> In this model, a rigorous self-consistency was applied which resulted in a modification of the usual  $Q \cdot Q$  interaction. In the spherical nucleus, the GQR has degenerate  $K=0, 1, 2$  components, while the GMR is  $K=0$ . When ground-state deformation is introduced, the  $K=0, 1, 2$  components of the GQR split apart, and the GQR and GMR oscillations mix. Thus, there are two  $K=0$  states, the lower predominantly  $J^\pi=2^+$  but containing significant  $J^\pi=0^+$  strength and the upper mostly  $J^\pi=0^+$  with a small amount of  $J^\pi=2^+$  strength. In qualitative agreement with the data, the upper  $K=0$  component remains nearly at the unperturbed position of the GMR. The calculations of Zawischa *et al.* apparently do not correctly reproduce the unperturbed

GMR position and thus yield too large an apparent splitting. Elementary calculations suggest that approximately three-fourths of the  $0^+$  strength should remain in the upper component; the data suggest an approximately even distribution.

The apparent absence of the GMR in lighter nuclei is puzzling. For  $A \geq 90$ , a strong GMR is observed with a yield at  $0^\circ$  equal to or greater than the GQR. In <sup>64,66</sup>Zn, the observed GMR is substantially weaker than the GQR at  $0^\circ$  (see Fig. 4). In <sup>58</sup>Ni, only Bertrand *et al.*<sup>7</sup> (from an analysis of inelastic proton data) have reported a significant concentration of monopole strength. Unfortunately, they must first subtract not only the GQR but also the GDR which is almost coincident with the GMR. Additionally, in proton scattering, the angular distributions are featureless, increasing the difficulty of separating the GR peaks and the continuum. While Bertrand *et al.*'s results for <sup>58</sup>Ni are consistent with inelastic  $\alpha$  data for <sup>64,66</sup>Zn, comparable strength was not seen in <sup>58</sup>Ni in this work. DWBA predictions with a hydrodynamic model form factor suggest that the strength in inelastic  $\alpha$  scattering of the GMR should decrease somewhat relative to the GQR for lighter nuclei. For <sup>40</sup>Ca, using the experimental results in heavy nuclei and correcting for the  $A$  dependence with DWBA predictions, one would expect  $\sigma_0/\sigma_{2^+}(0^\circ) \approx 0.6$  if each depletes the same fraction of the respective sum rule. No candidate for such  $0^+$  strength is apparent in the data, as can be seen in Fig. 10. Measurements with protons,<sup>7</sup> deuterons,<sup>9</sup> <sup>3</sup>He,<sup>20</sup> and alphas<sup>17</sup> are in substantial agreement on the absence of a GMR in <sup>40</sup>Ca. It has been known for some time that the GQR broadens and splits in lighter nuclei, due in part to the lack of enough closely spaced low-lying valence orbits to reproduce the truly collective GQR seen in heavier nuclei. Perhaps the GMR is behaving in a similar fashion with the strength spreading even more broadly in light nuclei than is the case with the GQR. Alternately, since the GMR and GQR energies change somewhat differently with  $A$ , it is conceivable that they are almost coincident in lighter nuclei and the present experiments have simply not distinguished them. Moreover, there is no good test yet of the reaction theory for the GMR, and, perhaps, the excitation of the GMR in light nuclei is weaker than predicted. Further experimental and theoretical effort will be required to ascertain what happens to the GMR in light nuclei.

This work was supported in part by the National Science Foundation and the Robert A. Welch Foundation.

- \*Present address: Harshaw Chemical Company, Solon, Ohio 44139.
- <sup>1</sup>N. Marty, M. Morlet, A. Willis, V. Comparat, and R. Frascaria, in *Proceedings of the International Symposium on Highly Excited States in Nuclei, Jülich, 1975*, edited by A. Faessler, C. Mayer-Böricke, and P. Turek (Kernforschungsanlage, Jülich GmbH, Germany, 1975), Vol. I, p. 17.
- <sup>2</sup>S. Fukuda and Y. Torizuka, *Phys. Lett.* **62B**, 146 (1976); M. Sasao and Y. Torizuka, *Phys. Rev. C* **15**, 217 (1977).
- <sup>3</sup>M. N. Harakeh, K. van der Brog, T. Ishimatsu, H. P. Morsch, A. van der Woude, and F. Bertrand, *Phys. Rev. Lett.* **13**, 676 (1977); M. N. Harakeh, B. van Heyst, K. van der Borg, and A. van der Woude, *Nucl. Phys.* **A327**, 373 (1979).
- <sup>4</sup>D. H. Youngblood, C. M. Rozsa, J. M. Moss, D. R. Brown, and J. D. Bronson, *Phys. Rev. Lett.* **39**, 1188 (1977).
- <sup>5</sup>C. M. Rozsa, D. H. Youngblood, J. D. Bronson, Y.-W. Lui, and U. Garg, *Phys. Rev. C* **21**, 1252 (1980).
- <sup>6</sup>Y.-W. Lui, P. Bogucki, J. D. Bronson, U. Garg, C. M. Rozsa, and D. H. Youngblood, *Phys. Lett.* **93B**, 31 (1980).
- <sup>7</sup>F. E. Bertrand, G. R. Satchler, D. J. Horen, and A. van der Woude, *Phys. Rev. C* **18**, 2788 (1978); *Phys. Lett.* **80B**, 198 (1979).
- <sup>8</sup>M. Buenerd, C. Bonhomme, D. Lebrun, P. Martin, J. Chauvin, G. Duhamel, G. Perrin, and P. de Saintignon, *Phys. Lett.* **84B**, 305 (1979).
- <sup>9</sup>A. Willis, M. Morlet, N. Marty, R. Frascaria, C. Djallali, V. Comparat, and P. Kitching, *Nucl. Phys.* **A344**, 137 (1980).
- <sup>10</sup>J. P. Blaizot, D. Gogny, and B. Grammaticos, *Nucl. Phys.* **A265**, 315 (1976).
- <sup>11</sup>O. Bohigas, A. M. Lane, and J. Martorell, *Phys. Rep.* **51**, 267 (1979).
- <sup>12</sup>A. M. Bernstein, *Adv. Nucl. Phys.* **3**, 325 (1969).
- <sup>13</sup>G. R. Satchler, *Nucl. Phys.* **A100**, 497 (1967).
- <sup>14</sup>J. Mathews and R. L. Walker, *Mathematical Methods of Physics*, 2nd ed. (Benjamin, New York, 1970), p. 387.
- <sup>15</sup>D. H. Youngblood, J. M. Moss, C. M. Rozsa, J. D. Bronson, A. D. Bacher, and D. R. Brown, *Phys. Rev. C* **13**, 994 (1976).
- <sup>16</sup>U. Garg, P. Bogucki, J. D. Bronson, Y.-W. Lui, C. M. Rozsa, and D. H. Youngblood, *Phys. Rev. Lett.* **45**, 1670 (1980).
- <sup>17</sup>Y.-W. Lui, J. D. Bronson, C. M. Rozsa, D. H. Youngblood, P. Bogucki, and U. Garg (unpublished).
- <sup>18</sup>P. de Saintignon, P. Martin, M. Buenerd, D. Lebrun, J. Chauvin, and G. Perrin, in *Giant Multipole Resonances*, edited by F. E. Bertrand (Harwood, New York, 1980), p. 464.
- <sup>19</sup>H. Rost, W. Eyrich, A. Hofmann, U. Scheib, and F. Vogler, *Phys. Lett.* **88B**, 51 (1979).
- <sup>20</sup>T. Yamagata, K. Iwamoto, S. Kishimoto, B. Saeki, K. Yuasa, M. Tanaka, T. Fukuda, K. Okada, I. Miura, M. Inoue, and H. Ogata, *Phys. Rev. Lett.* **40**, 1628 (1978).
- <sup>21</sup>D. H. Youngblood, C. M. Rozsa, J. M. Moss, D. R. Brown, and J. D. Bronson, *Phys. Rev. C* **15**, 1644 (1977).
- <sup>22</sup>C. M. Lederer and V. S. Shirley, *Table of Isotopes*, 7th ed. (Wiley, New York, 1978).
- <sup>23</sup>M. Buenerd, D. Lebrun, J. Chauvin, P. Martin, G. Perrin, and P. De Saintignon, in *Giant Multipole Resonances*, edited by F. E. Bertrand (Harwood, New York, 1980), p. 437.
- <sup>24</sup>H. P. Morsch, C. Sükösd, M. Rogge, P. Turek, H. Machner, and C. Mayer-Böricke, *Phys. Rev. C* **22**, 489 (1980).
- <sup>25</sup>B. K. Jennings and A. D. Jackson, *Nucl. Phys.* **A342**, 23 (1980).
- <sup>26</sup>D. Zawischa, J. Speth, and D. Pal, *Nucl. Phys.* **A311**, 445 (1978).
- <sup>27</sup>T. Kishimoto, J. M. Moss, D. H. Youngblood, J. D. Bronson, C. M. Rozsa, D. R. Brown, and A. Bacher, *Phys. Rev. Lett.* **35**, 552 (1975); T. Kishimoto (private communication).